Mesoscopic Structure in the Chain-Melting Regime of Anionic Phospholipid Vesicles: DMPG

K. A. Riske,* L. Q. Amaral,[†] H.-G. Döbereiner,*[‡] and M. T. Lamy[†]

*Max Planck Institute of Colloids and Interfaces, Theory Department, Am Mühlenberg, Golm, Germany; [†]Instituto de Física da Universidade de São Paulo, São Paulo, Brazil; and [‡]Department of Biological Sciences, Columbia University, New York, New York

ABSTRACT   In a range of low ionic strength, aqueous dispersions of the anionic phospholipid DMPG (dimyristoylphospha-tidylglycerol) have a transparent intermediate phase (IP, between $T_m^{on} \cong 20°C$ and $T_m^{off} \cong 30°C$) between the turbid gel and fluid membrane phases, evidenced in turbidity data. Small angle x-ray scattering results on DMPG dispersions show that, besides the bilayer peak present in all phases, a peak corresponding to a mesoscopic structure at ~400 Å is detected only in IP. The dependence of this peak position on DMPG concentration suggests a correlation in the bilayer plane, consistent with the stability of vesicles in IP. Moreover, observation of giant DMPG vesicles with phase contrast light microscopy show that vesicles "disappear" upon cooling below T_m^{off} and "reappear" after reheating. This further proves that although vesicles cannot be visualized in IP, their overall structure is maintained. We propose that the IP in the melting regime corresponds to unilamellar vesicles with perforations, a model which is consistent with all described experimental observations. Furthermore, the opening of pores across the membrane tuned by ionic strength, temperature, and lipid composition is likely to have biological relevance and could be used in applications for controlled release from nanocompartments.

INTRODUCTION

The so-called main phase transition of lipid bilayers has been extensively studied over the last decades, both because of its biological relevance, and for its intrinsic interest as a fundamental problem in the physics of membranes. The chain-melting transition, occurring at a temperature T_m, corresponds to a defined change from a state of ordered (gel state) to disordered (fluid state) hydrocarbon chains (Luzzati, 1968; Nagle, 1980). The majority of the studies on the melting transition of lipids have been performed on pure neutral phosphatidylcholines (Nagle and Wilkinson, 1978; Koynova and Caffrey, 1998, and references therein; Nagle and Tristram-Nagle, 2000) or on mixtures of different lipids (Van Dijck et al., 1977; Silvius, 1986; Mason, 1988; Bagatolli and Gratton, 2000). For lipid mixtures the phase rule allows a temperature interval in which water may be in equilibrium with gel and fluid lipid domains (Chernik, 1995). Since most cell membranes have a net negative charge, studies on mixtures of neutral and charged phospholipids are receiving increased attention. The main transition of charged single-component lipid bilayers, as well as its dependence on ionic strength and pH, is therefore of key relevance to understand phase transitions in mixtures.

In this article we draw attention to dispersions of pure anionic phospholipids, which can exhibit a ''melting re-gime'' (temperature interval where the melting process evolves) instead of a unique melting transition. In particular, this melting regime was investigated for dimyristoylphos-phatidylglycerol (DMPG), whose aqueous dispersions have unusual physicochemical properties under different condi-tions of pH, ionic strength, lipid concentration and time of incubation at low temperatures (Watts et al., 1978; Epand and Hui, 1986; Gershfeld et al., 1989; Salonen et al., 1989; Epand et al., 1992; Heimburg and Biltonen, 1994; Zhang et al., 1997; Riske et al., 1997, 1999, 2001, 2002, 2003a; Schneider et al., 1999; Lamy-Freund and Riske, 2003). Specifically, the melting regime is observed in a wide range of DMPG concentrations (at least between 0.1 and 100 mM; Riske et al., 2002, 2003b) for pH values above 5, where the phosphate groups are deprotonated, and for salt concentrations below 100 mM, where charge screening is weak. Electron spin resonance (ESR) spectra of spin labels intercalated in the bilayer show that the chain-melting process starts at T_m^{on} (onset of the melting regime at ~20°C), but a fluid phase exists only above T_m^{off} (offset of the melting regime at ~30°C; Riske et al., 2001). Differential scanning calorimetry (DSC) gives a sequence of endothermic peaks, between a sharp peak at T_m^{on} and a broad one at T_m^{off} (Riske et al., 2001). Both ESR and DSC data are reversible with temperature and do not depend on equilibration time. Intriguingly, the melting regime of low ionic strength DMPG is coupled to large changes in sample turbidity (Heimburg and Biltonen, 1994; Riske et al., 1997). Whereas the gel and fluid phases are turbid, the sample is completely transparent in the melting regime. This suggests that a new phase is formed in the melting regime. This phase was named the intermediate phase (IP), since it appears between the gel and fluid phases. An abrupt and dramatic decrease in sample turbidity occurs at T_m^{on}, which is then partially recovered at T_m^{off}. The smaller difference in turbidity between the gel and fluid phases is

consistent with the measured variation of the refractive index increment in the main phase transition (15%; Riske et al., 1997). The open question is the origin of the dramatic drop in turbidity in the IP. The refractive index of the sample in IP decreases continuously from the gel to the fluid phase, without showing a minimum that could explain the one observed in the turbidity curve (Riske et al., 1997). A review of such studies is found in Lamy-Freund and Riske, 2003.

In a previous work (Riske et al., 2001), we studied DMPG dispersions using small angle x-ray scattering (SAXS) down to $q \cong 0.03$ Å^{-1} (q being the scattering vector modulus given by $q = 4\pi \, (\sin \theta)/\lambda$, where 2θ is the scattering angle and λ is the wavelength). A broad peak was detected in all phases, consistent with the scattering expected for large unilamellar vesicles. No Bragg peak characteristic of multilamellar vesicles was observed, since charged phospholipids generally avoid forming ordered multilamellae due to electrostatic repulsion. The broad peak could be well fitted by a single bilayer form factor, with changeable bilayer thickness and electron density contrast (Riske et al., 2001). A decrease in the peak intensity occurs within the IP. Furthermore, the peak position moves to larger q values due to the decrease in bilayer thickness with temperature. SAXS curves could be modeled assuming an anomalous decrease in electron density contrast, proposed to correlate with a separation of the charged headgroups in the IP (Riske et al., 2001).

Here we report new x-ray results, with the q range extended to both smaller and larger values, reaching the wide angle region (WAXS). The latter provides information on the hydrocarbon chain array. At very low angles a new peak could be detected only in the IP, corresponding to a mesoscopic structure around 400 Å. The lipid concentration has also been varied (from 10 to 80 mM DMPG) to define the origin of this new peak. Together with new results on phase contrast light microscopy of giant DMPG vesicles along the same phase transitions, we are now able to propose a structure for the DMPG vesicles within the melting regime.

MATERIALS AND METHODS

Materials

The sodium salt of DMPG (1,2-dimyristoyl-*sn*-glycero-3-[phospho-*rac*-glycerol]) was purchased from Avanti Polar Lipids (Birmingham, AL) and was used without further purification. Purity is checked by the re-producibility of T_{m}^{on} on a standard sample preparation.

Lipid dispersion preparation

A lipid chloroform solution (200 μl of 10–80 mM DMPG, depending on the desired lipid concentration) was prepared and dried under a stream of N$_2$, so as to form a homogeneous lipid film in the walls of a glass tube. The tube was left under vacuum overnight to remove all traces of the organic solvent. Vesicle dispersions were prepared by adding 200 μl 10 mM HEPES pH 7.4 + 2 mM NaCl, and vigorously vortexing for ~2 min above T_{m}^{off}. The measurements were always done with samples prepared on the same day, when lipid isomerization and/or degradation are not expected to happen. The

concentration obtained from weighed components agrees with the concentration measured by phosphate counting.

Turbidity measurements

Sample turbidity (absorbance at $\lambda = 350$ nm and 2 mm optical path) was measured on 50 mM DMPG at low ionic strength (10 mM HEPES , pH 7.4, + 2 mM NaCl) with a HP 8452A diode array spectrophotometer (Hewlett-Packard, Palo Alto, CA). Temperature was adjusted with a circulating water bath.

Preparation and observation of giant vesicles

Giant vesicles were prepared by electroformation (Angelova and Dimitrov, 1986). Briefly, a few drops of a 10 mg/ml DMPG chloroform solution were spread on the surface of two electrodes. The electrodes stayed under vacuum for at least 1 h to remove all traces of the organic solvent, and were then placed inside a visualization chamber. The whole chamber was in contact with a water bath set at 40°C (above T_{m}^{off}). The alternating electric field was set to 1.5 V with a 10-Hz frequency. The chamber was then filled with 10 mM HEPES, pH 7.4, + 2 mM NaCl (~1.5 ml). After a few minutes, giant vesicles started to grow from the surface of the electrodes. The chamber was observed under an inverted Axiovert 135 Zeiss microscope (Oberkochen, Germany) equipped with a 40 × Ph2 objective.

Small angle x-ray scattering

The measurements were done in the SAXS beam line of the LNLS (National Laboratory of Synchrotron Radiation, Campinas, SP, Brazil.). The x-ray wavelength used was $\lambda = 1.608$ Å. The SAXS sample detector distance varied in the range 90–180 cm. A SAXS-WAXS camera was used in some of the measurements for the simultaneous detection of the wide-angle diffraction. A linear position-sensitive detector and an image plate detector were used for SAXS and WAXS, respectively. A thermal bath was used for temperature variation. Samples were conditioned in a sample holder with flat Mylar walls and 1-mm thickness. Data were normalized for the acquisition time (10–20 min), monitor integral counts (to compensate for oscillations in the beam intensity), sample attenuation, and DMPG concentration, and corrected for the SAXS detector response (measured with a radioactive source). The measured scattering due to the buffer, which has no structure in the SAXS region and the well-known water band ~2 Å^{-1} in the WAXS region (Hura et al., 2003), were subtracted from all scattering curves.

RESULTS

SAXS and WAXS

Dispersions of 50 mM DMPG in 10 mM HEPES + 2 mM NaCl have been investigated using both a SAXS-WAXS camera and a SAXS setup. According to previous results (Riske et al., 2001), this specific DMPG condition has transition temperatures $T_{m}^{on} = 19$°C and $T_{m}^{off} = 30–35$°C (depending on preparation/batch, possibly due to small variations in salt contamination. The use of 2 mM NaCl was adopted to decrease such effects). At least three independently prepared samples were investigated in each experimental arrangement, showing clear data reproducibility. Moreover, all results were shown to be reversible upon heating and cooling cycles, with only small variation in the value of T_{m}^{off}. Typical results obtained with one of the samples in the SAXS-WAXS camera are shown in Figs. 1 and 2.
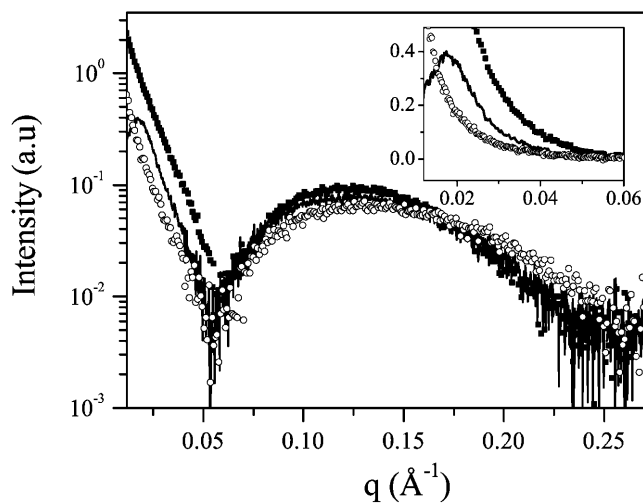
FIGURE 1 SAXS curves obtained for 50 mM DMPG in 10 mM HEPES, pH 7.4, + 2 mM NaCl at 9°C (■), 25°C (*line*), and 37°C (○), corresponding to the gel, intermediate, and fluid phases, respectively. The inset shows a magnification of the low q region, to call the attention to the peak at q_1, present only in IP.

Normalized SAXS intensity curves, $I(q)$, for three different temperatures (corresponding to the gel, intermediate, and fluid phases) are displayed in Fig. 1. The peak at $q_{max} \cong 0.12$ Å^{-1} is due to single bilayers, arising from electron density differences between the inside of the bilayer and the solvent, as already discussed (Riske et al., 2001). A new peak (see inset of Fig. 1) is now detected around $q_1 \cong 0.017$ Å^{-1} (characteristic distance $2\pi/q_1 \cong 370$ Å), present over the whole temperature range of the IP, which changes sharply both at T_m^{on} and T_m^{off}. On the other hand, the bilayer peak starts to change continuously at T_m^{on} and changes sharply only at T_m^{off} (Riske et al., 2001). This peak at low q values is the first direct evidence of structural changes at the supramolecular level in the IP, since freeze-fracture electron
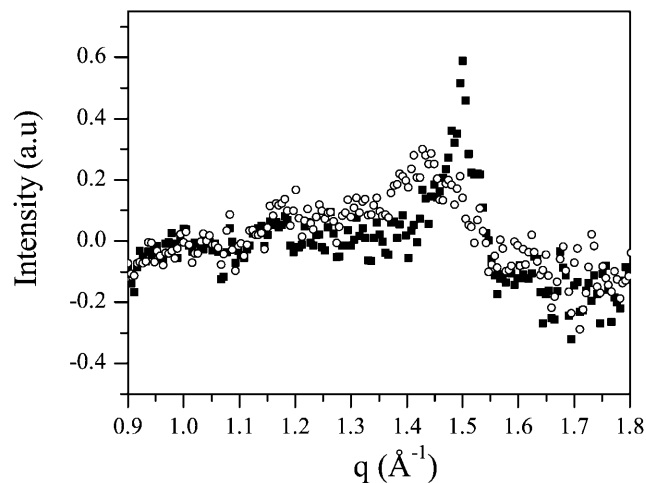

FIGURE 2 WAXS curves obtained at 15°C (■, gel phase) and 23°C (○, IP).

micrographs obtained by other authors (Watts et al., 1978; Schneider et al., 1999) cannot completely assure that the structure of IP is kept during the quench process.

Fig. 2 shows WAXS results for temperatures below and above T_m^{on} (gel and intermediate phase, respectively). The statistics are not very good after subtraction of the buffer scattering, because the hydrocarbon chains represent <1% of the sample volume and their WAXS peak at ~1.5 Å^{-1} overlaps with the dominant water band at ~2 Å^{-1}. Nevertheless, a clear change between the gel phase and the IP could be detected in three independently prepared samples. A sharp peak at 1.5 Å^{-1} due to ordered acyl chains is seen only below T_m^{on} and is replaced by a broad band ~1.4 Å^{-1} above T_m^{on}. This change is in accordance with what is expected for the gel and fluid phases, respectively (Luzzati, 1968). It can be concluded that the long-range order of the chains typical of the gel phase disappears at T_m^{on}, where a sharp endothermic peak is detected in the DSC run (Riske et al., 2001). There might be some further changes along IP and at T_m^{off} (WAXS curves not shown), but they could not be clearly detected. WAXS results are in agreement with DSC and ESR results (Riske et al., 2001), which show a marked change at T_m^{on}, although smaller changes continue to occur until T_m^{off}.

Fig. 3, *a–d*, displays the temperature variation of the position and intensity of the bilayer peak (q_{max}, I_{max}) and the IP peak (q_1, I_1) in a particular sample carefully investigated by SAXS in a heating-cooling-heating cycle, starting and finishing at room temperature (for this specific sample $T_m^{off} = 35°C$). Except when indicated, points are averages over heating and cooling scans. The bilayer peak position q_{max} increases continuously along IP (Fig. 3 *a*). Its intensity I_{max} (Fig. 3 *b*) starts to decrease at T_m^{on}, reaches a minimum at 34°C (just below T_m^{off}), and partially recovers its intensity above T_m^{off}. The minimum below T_m^{off} is difficult to reproduce and requires variation of the temperature in very small steps, as done previously (Fig. 4 of Riske et al., 2001). In this sample the minimum was better defined upon heating, possibly due to a small change in T_m^{off} in the heating-cooling process. The IP peak at q_1 appears at T_m^{on}, reaches a maximum value at ~25°C, and disappears at T_m^{off} (Fig. 3 *c*), whereas its intensity I_1 shows a minimum around 29°C (Fig. 3 *d*). Both I_{max} and I_1 have a minimum in IP, but at different temperatures. This indicates that the two peaks cannot arise from a simple single form factor. None of the peak intensities follows an exponential or linear decay.

To investigate the origin of the IP peak, samples with DMPG concentration in the interval 10–80 mM were measured (with 10-mM steps). Fig. 4 shows the q_1 region of normalized SAXS curves (corrected intensity divided by concentration) obtained for 20, 30, 40, 50, and 60 mM DMPG at 25°C (in IP). For 20 and 30 mM DMPG only a change in curvature in the low q region was detected and the point of inflection was taken as q_1. The same trend, but with poor statistics, was obtained for 10 mM DMPG. For 50 and 60 mM DMPG, the peaks are clearly defined and their
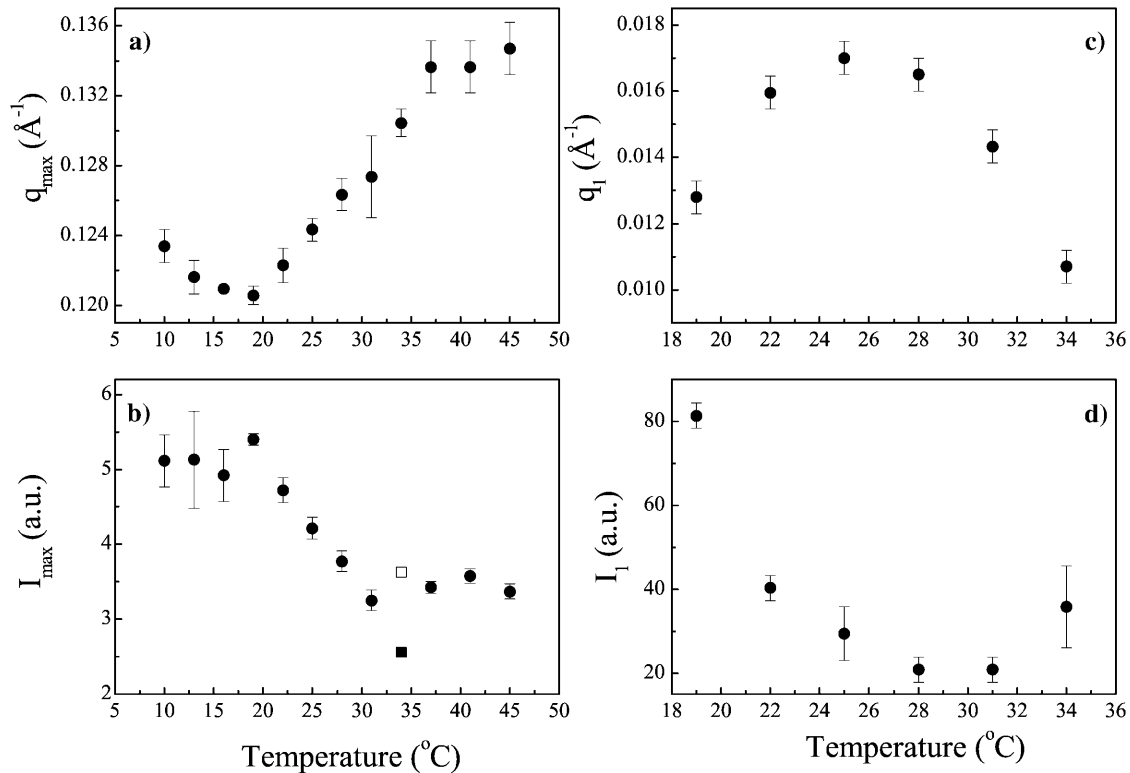
FIGURE 3 Temperature variation of (*a*) bilayer peak position (q_{max}); (*b*) bilayer peak intensity (I_{max}); (*c*) IP peak position (q_1); and (*d*) IP peak intensity (I_1). Results measured from SAXS curves of 50 mM DMPG in 10 mM HEPES, pH 7.4, + 2 mM NaCl. The data shown are an average of heating/cooling scans (●; difference between them defines the error bars). The only exception is I_{max} at 34°C (*b*), where the values obtained upon heating (■) and upon cooling (□) are explicitly shown and discussed in the text.

intensities coincide. The result for 40 mM DMPG is intermediate. All the concentrations join at ~0.018 Å^{-1}, and for higher q values there are no concentration effects. The peak position q_1 increases slightly with concentration, as shown in Fig. 5 *a*. These details, along with Fig. 5 *b*, will be

addressed further in the Discussion section. SAXS curves obtained for higher DMPG concentration showed a co-existence with another superstructure in the temperature region of the IP at ~70 mM DMPG. A broad peak at ~0.017 Å^{-1} is still detected above T_m^{on} in the 70-mM sample, similar to the one detected in 50 and 60 mM DMPG. However, it becomes sharper within the IP with temperature and/or time, indicating a more defined long-range order but a rather complex behavior at higher concentrations. Furthermore, for 80 mM DMPG the intensity below 0.02 Å^{-1} drops by a factor of 2 in relation to 50 and 60 mM, a typical effect of interaggregate interference. There is therefore strong evidence of a transition to another superstructure around 70 mM, with possible destruction of vesicles. These structures (which may be metastable) are out of the scope of this article. Our aim is to unravel the stable IP up to 70 mM DMPG. Possible origins for the observed peak at q_1 will be discussed further on.
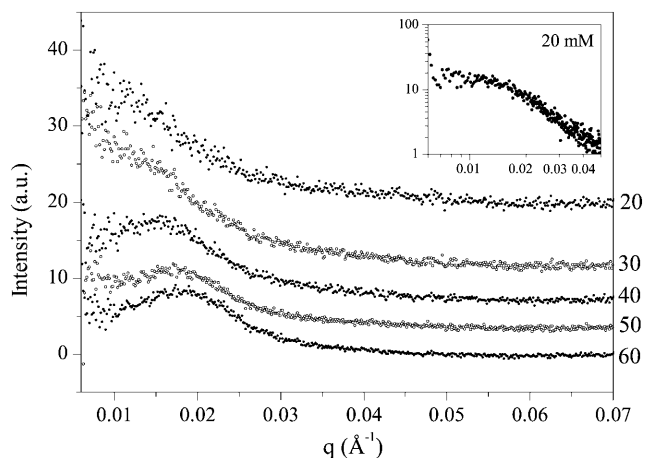

FIGURE 4 SAXS curves obtained for 20, 30, 40, 50, and 60 mM DMPG in 10 mM HEPES, pH 7.4, + 2 mM NaCl. The curves are shifted to help visualization. The curve at 20 mM DMPG is shown in the inset in a log-log scale to evidence the change in curvature defining q_1.

Optical microscopy and turbidity

DMPG dispersions were observed under a phase contrast light microscope. According to previous static light-scattering measurements, the average vesicle diameter in
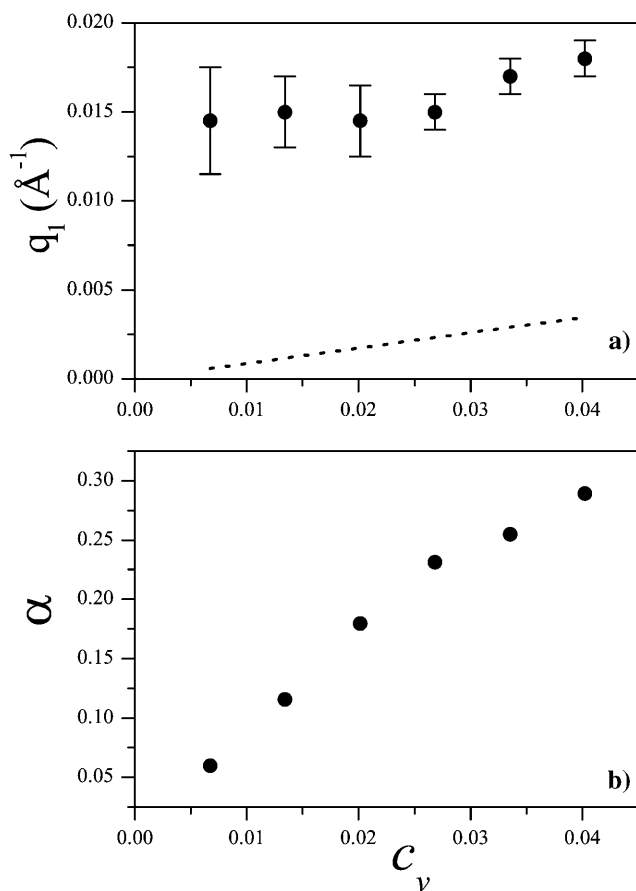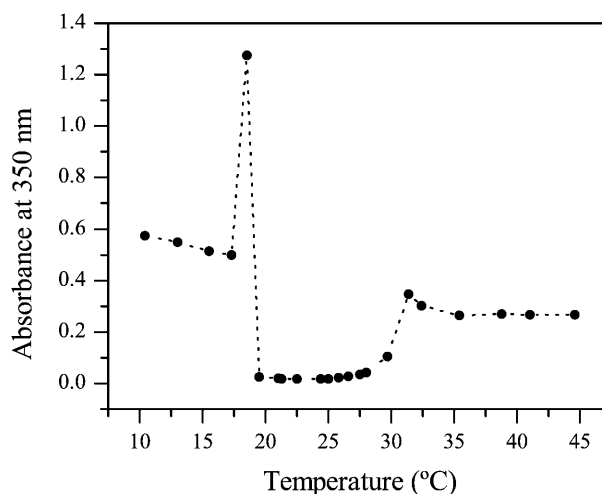
FIGURE 6   Turbidity (measured as sample absorbance at 350 nm with 2-mm optical path) of 50 mM DMPG in 10 mM HEPES, pH 7.4, + 2 mM NaCl as a function of temperature. The line connecting the experimental points is just a guide for the eyes.

FIGURE 5   (*a*) Variation of q_1 with the volume fraction c_v in the interval 10–70 mM DMPG at 25°C (●). The line shows the expected values for the case of a sponge phase ($\alpha = 1.5$). (*b*) Corresponding α values obtained from Eq. 3.

the gel and fluid phases is of the order of 10^3 Å (Riske et al., 1997), too small for vesicles to be individually seen by light microscopy. However, a texture of small vesicles can be seen below T_m^{on} (gel phase) and above T_m^{off} (fluid phase). On the other hand, the sample is completely transparent within the IP. This observation parallels the turbidity data, shown in Fig. 6 for a 50 mM sample as the one used in most of the x-ray measurements. The sample is turbid in the gel and fluid phases, and transparent in the IP, as previously reported for smaller concentrations (Riske et al., 1997). Abrupt changes in turbidity occur both at T_m^{on} and T_m^{off}. The increase in intensity at 18.5°C (just below $T_m^{on} = 19$°C) will be discussed further on.

To visualize single DMPG vesicles by optical microscopy, giant vesicles (radii ~10 μm) were grown by electroformation in the fluid phase. Fig. 7 shows a sequence of images of a single giant vesicle along one temperature cycle through T_m^{off} (for this sample $T_m^{off} = 28$°C). The first snapshot shows the giant vesicle in the fluid phase. Upon cooling, the vesicle vanishes as T_m^{off} is crossed, and reappears when the temperature is increased again above T_m^{off}. Four consecutive

temperature cycles through T_m^{off} were performed and the same vesicle was always observed in the fluid phase. This shows with certainty that the vesicle structure is preserved in the IP, since giant DMPG vesicles are not spontaneously formed as a result of crossing T_m^{off}. This behavior is also shown for a collection of vesicles in Fig. 8. All vesicles vanish around T_m^{off} upon cooling, and reappear after reheating the sample. In all experiments performed, the whole collection of vesicles disappears below T_m^{off}. The vanishing of the vesicles was certainly not an artifact due to vesicle drift out of the viewing area (caused by the change in temperature), since the whole chamber was scanned and the focal plane has been changed: the sample is completely transparent in the IP. Furthermore, it is clear from the pictures shown at T_m^{off} that the vesicles vanish gradually (piece by piece), and no vesicle movement whatsoever is seen. However, if the sample is maintained more than 15 min in the IP, giant vesicles are no longer seen either above T_m^{off} or below T_m^{on}, and only a texture of small vesicles is observed (as seen with the dispersions). This indicates that the giant vesicles eventually break into smaller ones within the IP. Yet, it is important to say that vesicle destabilization happens only with giant vesicles, since dynamic light-scattering data of DMPG dispersions shows that the mean vesicle radius is maintained constant both in the fluid and gel phases, irrespective of the number of cycles through IP. Furthermore, lipid rearrangement does not happen across these transitions or along IP, as demonstrated by ESR experiments (Riske et al., 1999). It is also very important to stress that both giant vesicles and the texture of small vesicles appear and disappear at the same temperature. This can be seen in Fig. 8, where many giant vesicles coexist with a texture of small vesicles (marked with an *asterisk*). Thus, the loss in contrast of the giant vesicles shown in Figs. 7 and 8 is a general
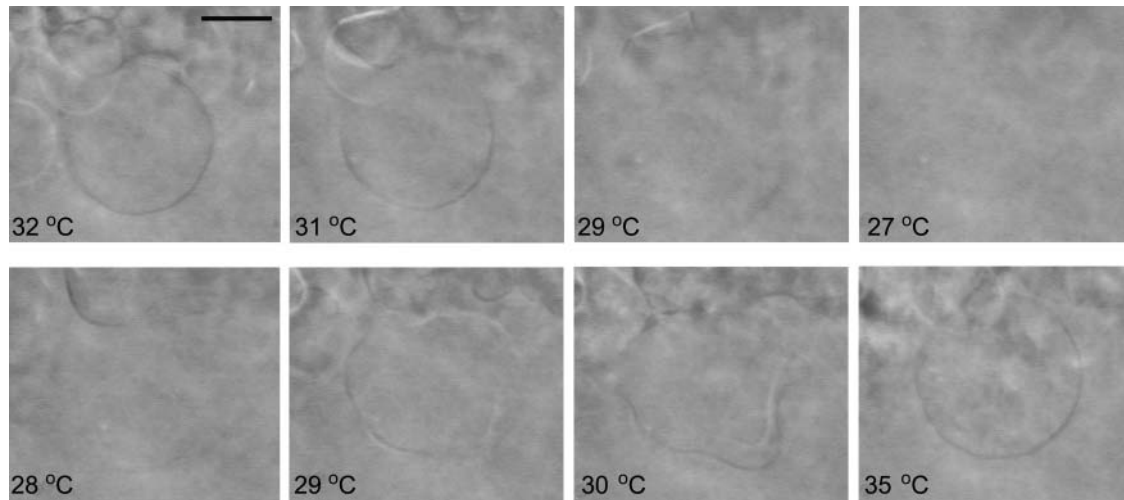
FIGURE 7   Sequence of pictures obtained by phase contrast microscopy of one and the same giant DMPG vesicle in 10 mM HEPES, pH 7.4, + 2 mM NaCl along one temperature cycle through $T_m^{off} \cong 28°C$. The time interval between the pictures was 30–60 s. The bar denotes 10 μm.

feature of DMPG bilayers, irrespective of the size of the vesicles they form. It is clear that the loss in bilayer contrast occurs within the bilayer itself, not requiring the breaking of the vesicle structure, as shown in Fig. 7.

DISCUSSION

Analysis of SAXS curves

In the previous article (Riske et al., 2001) SAXS curves in the interval 0.03–0.35 Å^{-1} were well fitted using the form factor of a single bilayer, according to Glatter and Kratky (1982):

$$I(q) = N(2\pi/q^2)F_t^2(q), \qquad (1)$$

where N is a normalization constant and $F_t(q)$ is the bilayer transversal form factor, given by

$$F_t(q) = \int_{-t/2}^{+t/2} \rho(x)\cos(qx)dx, \qquad (2)$$

where $\rho(x)$ is the electron density profile in the direction perpendicular to the bilayer plane and t is the bilayer thickness. The q^{-2} factor in Eq. 1 is a fingerprint of planar symmetry.

A step model was used, where $\rho(x)$ is described by three levels representing the headgroups (ρ_1), the alkyl chains (ρ_2) and the methyl groups (ρ_3), with widths R_1, R_2, and R_3, respectively. Even though real bilayers do not show sharp steps in $\rho(x)$, the step model yields a reasonable fit to the data (Wiener et al., 1989, 1991). Such a model has the meaning of an effective profile that mimics the membrane. For neutral lipids, the main phase transition has been found to basically induce a decrease in the thickness of the bilayer and a small decrease in the electron density of the alkyl chains and
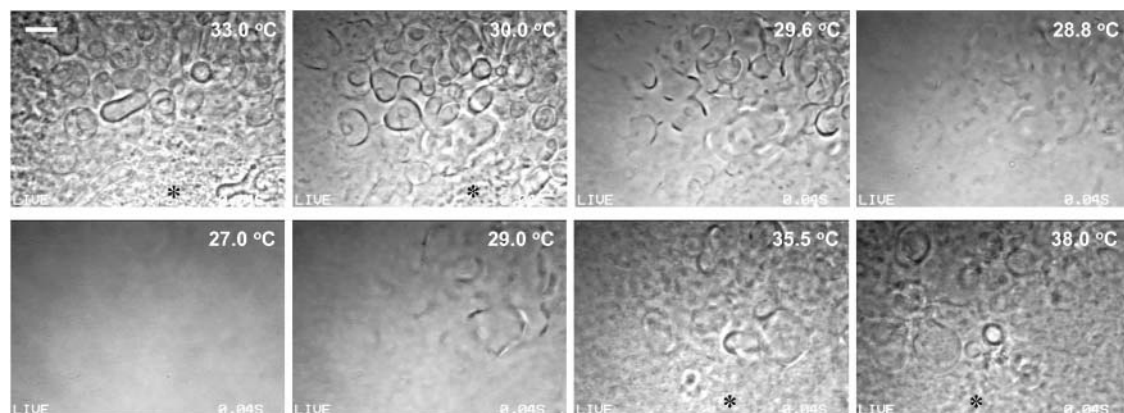

FIGURE 8   Sequence of pictures obtained by phase contrast microscopy of a collection of giant DMPG vesicles in 10 mM HEPES, pH 7.4, + 2 mM NaCl along one temperature cycle through $T_m^{off} \cong 28°C$. The giant vesicles coexist with a texture of small vesicles, marked with an asterisk. The time interval between the pictures was 30–60 s. The bar denotes 10 μm.

TABLE 1

	R_1 (Å)	R_2 (Å)	R_3 (Å)	t (Å)	ρ_1 (e/Å³)*	ρ_2 (e/Å³)*	ρ_3 (e/Å³)*
			SAXS data from Riske et al., 2001				
10°C	10.0	12.8	3.3	52.2	0.46	0.32	0.21
27°C	10.0	12.1	3.0	50.2	0.40	0.32	0.25
35°C	10.0	8.9	3.5	44.8	0.45	0.29	0.19
			New SAXS data, Fig. 9				
9°C	10.0	12.8	3.3	52.2	0.46	0.32	0.21
28°C	10.0	12.1	3.3	50.8	0.43	0.32	0.21
37°C	10.0	9.0	3.5	45.0	0.44	0.30	0.21

Parameters used in the fittings (Eqs. 1 and 2) of SAXS curves: thickness (R) and electron density (ρ) of the headgroup (1), alkyl chain (2), and methyl group (3) bilayer regions. The total bilayer thickness, $t = 2 (R_1 + R_2 + R_3)$, is also given. The first set of data (10, 27, and 35°C) refers to a previous work (Riske et al., 2001) and the second set (9, 28, and 37°C) was obtained in this work. The same normalization constant N (Eq. 1) was used for each set of data. The estimated errors are 0.01 (e/Å³) in the electron density and 0.2 Å in the thickness.

*Absolute values were obtained considering the water electron density $\rho_w = 0.33$ e/Å³ (Nagle et al., 1996) and fixing the methylene electron density in the gel phase at $\rho_2^{gel} = 0.32$ e/Å³ (Wiener et al., 1989).

headgroups. Since the model has several parameters, the fitting is not unique and the choice of a good solution is defined by constraints on acceptable ranges, defined from previous knowledge of membrane structure, and a qualitative analysis of the global fitting. Also, the χ^2 of the fits has no absolute meaning. It depends on the arbitrary normalization constant N, since the SAXS curves are not in absolute units.

Table 1 shows the parameters previously obtained (Riske et al., 2001). The curves at 10°C and 35°C were fitted with parameter values typical of gel and fluid phases, respectively (as described in detail in Riske et al., 2001), with a decrease in the hydrocarbon chain thickness. The curve at 27°C, in the IP, was fitted with an intermediate hydrocarbon chain thickness in relation to the gel and fluid phases, but with an anomalous decrease in electron density contrast. Detailed analysis of fitting parameters as a function of temperature within IP, with so many parameters, is unable to give trustworthy information, because the basic process is unknown. But a clear result, which was not emphasized in the previous article (Riske et al., 2001), is that the experimental curves in the IP cannot be fitted by a linear combination of the curves of gel and fluid phases, even with arbitrary fractions for each of the two components. This rules out the possibility of the IP being a simple mixture of gel and fluid domains.

The SAXS curves now obtained with an extended q range can be fitted with the same single bilayer model, except for the peak at q_1 in the IP. Fig. 9 shows results for the gel, intermediate, and fluid phases, where fits are obtained with very similar parameters as before (also shown in Table 1). Deviations between the experimental and calculated curves occur around the minimum ($\sim$0.05 Å^{-1}) for the curve at 9°C and are enhanced by the log scale necessary to visualize the

full intensity range over the extended q range. In the previous article the curves and fittings were shown in a linear scale, and it was mentioned that in the gel phase SAXS curves showed nonzero intensities at this minimum (Riske et al., 2001). Nevertheless, the correctness of the model regarding the existence of a single bilayer peak is clear. The possibility of multilamellar vesicles in excess water may be discarded since even two bilayers with a fixed amount of water between them would lead to interference peaks not present in the experimental curves, as tested by simulated scattering curves.

The curves shown for the gel and fluid phases have the typical planar factor q^{-2} down to the low q limit and the lower intensity in the fluid phase in comparison to the gel phase is due to the change in electron density contrast. For the IP, however, it is not possible to obtain a fit with a trivial unique form factor in the whole studied q range. This indicates that the low q-feature in the IP cannot be interpreted as a scattering minimum of the form factor around $q = \sim$0.009 Å^{-1} (as may be expected for monodisperse vesicles). Also, the form factor of anisotropic flat bilayers does not have a minimum at low q (Glatter and Kratky, 1982). The most likely explanation for the peak at $\sim q_1$ is that it arises from some type of interference, responsible also for the marked decay in intensity at very low q in the IP, not seen in the gel and fluid phases. Although $2\pi/q_1$ is in principle compatible with the distance between two charged bilayers in excess water, multilamellar vesicles can be discarded, as discussed before. Also, formation/destruction of multi-lamellar vesicles at, respectively, T_m^{on}/T_m^{off} can be discarded both on the basis of the micrographs of the giant vesicles (Figs. 7 and 8) and from the evidence that no vesicle fusion occurs at these transitions (Riske et al, 1999).

Some more information is given by parameters obtained from integration of $qI(q)$ and $q^2I(q)$ over the entire q range, now large enough to allow determination of the average chord length l_c, which replaces the concept of particle size (the whole vesicle is not seen in the measured q range) in the case of connected networks (Glatter and Kratky, 1982). The result for the $I(q)$ curves shown in Fig. 1 is 26 Å for the gel phase, 22 Å for the IP, and 20 Å for the fluid phase, in good agreement with the thickness of a monolayer as given by the parameters obtained from the fitting of the curves to a three-step function (Table 1). The resulting specific area (interface area per sample volume unit), using the obtained l_c values to estimate the slope at the origin of the correlation function, is 0.0050 Å^{-1} for the gel phase, 0.0060 Å^{-1} for the IP, and 0.0065 Å^{-1} for the fluid phase. These numbers are in agreement with the expected structural changes from the gel to the fluid phases, with intermediate values for the IP.

Results shown in Fig. 3 a (q_{max}) and Fig. 3 b (I_{max}) indicate the possibility of existence of critical phenomena. It is well known that the melting transition displays anomalous behavior when seen from the high-temperature fluid side, which has been associated with a critical temperature T^*
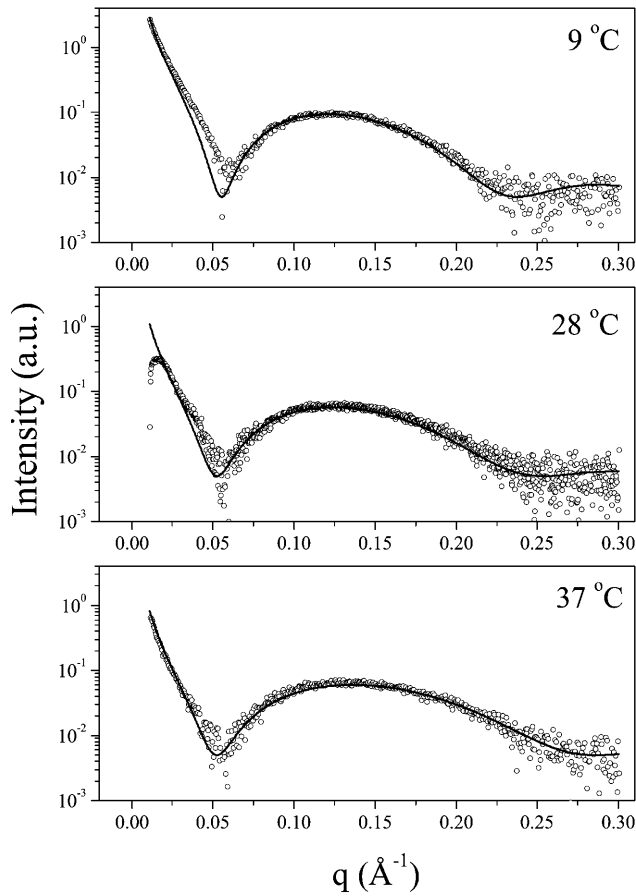
FIGURE 9 SAXS curves (○) and their respective fittings (*lines*). 50 mM DMPG in 10 mM HEPES + 2 mM NaCl at three temperatures: 9° (gel phase), 28° (IP), and 37°C (fluid phase). The curves at 9° and 37°C are the same ones shown in Fig. 1. The curve in the IP belongs to the same data series. We chose to fit the curve at 28°C because it yielded the maximum differences in the fitting parameters in comparison to the gel and fluid phases (listed in Table 1).

below the melting temperature T_m (Nagle, 1980). Most of such studies have been performed with multibilayer-forming phospholipids, and the repeat distance of the lamellar stack displays an anomalous swelling of controversial origin; a proposal of multiple mechanisms for the critical behavior has been presented (Nagle et al., 1998). Studies of the critical swelling in single phospholipid bilayers by neutron scattering (Mason et al., 2000) demonstrated that at least half of the anomalous swelling observed in multilamellar vesicles can be accounted for by critical thickening of the bilayer itself. The linear behavior of q_{max} in IP might indicate the existence of a critical temperature T^* practically coinciding with T_m^{on}. Exact analysis of critical exponents is hindered by the fact that neither the observed values q_{max} nor the zero position around 0.05 Å^{-1} give directly the bilayer thickness, since for x-ray scattering both depend also on the inner bilayer contrast. The turbidity curve in Fig. 6 shows just below T_m^{on}

a typical peak anomaly due to structural phase transitions and long-range correlation (Cummins and Levanyuk, 1983). This gives further evidence for the existence of a critical temperature slightly lower than T_m^{on}. It seems clear that the melting regime of DMPG might be related to the criticality proposed to exist in the normal melting behavior of phospholipids.

Analysis of the IP peak

When there is a homogeneous distribution of membranes in the solvent medium (lamellar phase, Luzzati, 1968), the average distance d between bilayer centers in the direction perpendicular to the bilayer plane is a function of the lipid volume fraction c_v in the bulk. The experimental lipid concentration c (in mM) is related to c_v through $c_v = 10^{-6} cMv$, where M is the molecular weight and v the partial specific volume of the lipid (for DMPG, v should be very similar to the one measured for DMPC (dimyristoylphosphatidylcholine): $v = 0.975$ ml/g in the fluid phase; Cevc, 1993).

For a bilayer, the symmetry decouples the three-dimensional volume partition of the lipid in a one-dimensional factor (perpendicular to the bilayer) and a two-dimensional factor (in the bilayer plane). For infinite planar bilayers with thickness t, c_v coincides with the linear fraction of lipid occupancy (t/d). When the lamellae have fluctuations or are finite, it is possible to define a lipid surface fraction α such that $c_v = \alpha(t/d)$. If the observed correlation peak at q_1 is due to the interlamellar spacing d it should therefore vary with c_v according to (Porte et al., 1989; Lei et al., 1997):

$$q_1 = 2\pi c_v/(t\alpha). \qquad (3)$$

The lipid surface fraction α is equal to 1 for a true lamellar phase. Bicontinuous or sponge phases without ripples have $\alpha = 1.5$ and the excess surface may be even larger when fluctuations occur in the lamellar plane. On the other hand, $\alpha < 1$ represents a deviation from the ''infinite'' lamellar structure, corresponding to disrupted infinite bilayers with holes, or independent bilayer fragments homogeneously distributed (or a combination of both). In the case of multilamellar vesicles in excess water the interlamellar distance is not a defined function of c_v, and the use of Eq. 3 leads to a nominal value $\alpha < 1$, which may vary with concentration.

The formation of a lipid network in the IP, without vesicles, has been proposed previously (Schneider et al., 1999). Fig. 5 *a* shows the expected value for q_1 if Eq. 3 were valid with $\alpha = 1.5$ and using $t = 50$ Å (total thickness, including headgroups, obtained from the fitting of the bilayer peak, shown in Table 1). The values thus obtained are much lower than the measured ones, evidencing that q_1 cannot be associated to a correlation, such as in a sponge phase. The value α can in fact be obtained from Eq. 3, using the

measured q_1 values. The result is $\alpha < 1$, growing with concentration, as seen in Fig. 5 *b*. The scattering curves exclude the possibility of multilamellar vesicles, as discussed in the previous section. The possibility of highly disrupted membranes or independent bilayer fragments, with a strong variation of the lipid surface fraction with concentration, cannot be completely ruled out. But such low α value, together with its almost linear variation with c_v, shows a complete deviation from the scaling behavior expected if q_1 were a correlation in the direction perpendicular to the bilayer plane. There is therefore an indication that q_1 should be better interpreted as coming from an in-plane correlation, and Eq. 3 is not valid. Furthermore, Eq. 3 precludes the existence of vesicles in the IP while the interpretation of q_1 as an in-plane correlation is compatible with the existence of vesicles in the IP, in agreement with the strong evidence in favor of the stability of vesicles over the whole temperature interval coming from the visualization of giant DMPG vesicles across T_m^{off} (Figs. 7 and 8).

We propose therefore that q_1 refers to a mesoscopic structure in the plane of the polar heads, which dominate the electron density contrast, with a correlation distance $D = 2\pi/q_1$. The distance d in the direction perpendicular to the bilayer would be much larger, corresponding to q values out of the observed range.

Proposed mesoscopic structure

The characteristic in-plane correlation distance D, together with the fact that there is a decrease in bilayer contrast, can be better understood considering $D = L + h$, corresponding to a disruption in the structure of the bilayer plane. L is the average size of a normal bilayer piece and h is a water pore. A picture of disrupted unilamellar vesicles with many pores or cavities, which may be punctual or linear, is thus obtained. Such a model is able to give a consistent picture for the IP of DMPG up to 70 mM, as discussed below.

The existence of perforations in lamellar phases, characterized by aqueous pores or cavities of several geometries surrounded by highly curved regions, has been shown in several systems with various techniques over the last two decades (Photinos and Saupe, 1984; Paz et al., 1984). The fingerprints of a disrupted membrane are in general an increase in conductivity and the existence of a large fraction of highly curved surface at the edges of the pores (Photinos and Saupe, 1984; Paz et al., 1984; Quist and Halle, 1993). The increase in conductivity is one of the characteristics of the IP (Riske et al., 1997). ESR results recently obtained with a spin probe labeled at the acyl chain end showed a characteristic spectrum only in the IP, with a two-peak feature in the high field region (Riske et al., 2003a). This spectrum is very likely due to the sum of two different spectra, representing spin labels in two distinct sites, which do not correspond to gel and fluid domains (a possibility that has been also excluded by x-ray results). One environment is

typical of bilayers, but with an intermediate mobility in respect to the gel and fluid phases, whereas the other is rather fluid and hydrated, resembling a micellar environment. These observations fit very well with the picture of bilayers with perforations. The more fluid and polar environment would correspond to spin labels located in the vicinities of the pores, whereas the other signal would correspond to spin labels residing in unperturbed bilayer regions. Assuming that the spin label is homogeneously distributed between the two environments, the ESR data indicated that approximately one-third of the DMPG molecules are in the more fluid and hydrated environment at 25°C. This fraction coincides with the population that would reside in the highly curved borders of a bilayer piece of area about $(L = 360 \text{ Å})^2$. This model is also able to account for the SAXS results obtained from the fitting of the bilayer peak (Table 1 and Fig. 9). Assuming $h = 10$ Å (minimum size of a hydrophilic pore; Glaser et al., 1988), and that the lipids are highly curved at the edges of the planar pieces, we obtain a decrease in the electron density contrast both in the headgroups and in the CH_3 regions, as discussed below. The positive contrast in the headgroup region is reduced because the perforations introduce water in the bilayer and the lipids at the highly curved edges of the pores do not contribute to the electron density on the plane of the bilayer headgroups. In the same way, the negative contrast in the CH_3 region is reduced due to the presence of headgroups in the cavities/pore walls and of water filling the channels. The magnitude of the decrease in contrast depends on the value of h and the detailed geometry of the pores. Estimates of the decrease are compatible with the electron density values obtained through the fitting of the SAXS curves shown in Table 1. Therefore, the decrease of contrast observed with temperature can be understood in terms of evolution of such disruption defects.

Fitting of the complete SAXS curves in the IP would require a detailed scattering theory of disrupted unilamellar vesicles, not yet available. A complete theory would need to unify the geometry of the cavities with its statistical distribution in the membrane surface.

The decay in sample turbidity (Fig. 6) and in optical contrast (Figs. 7 and 8) can be understood in terms of light passage through the cavities and/or pores. This results in a continuum of water, with interconnected bilayer pieces of ~300–400 Å. Such ''vesicles in pieces'' scatter much less light since the volume of the piece, which acts as the effective scattering particle, is a factor 10^{-4} smaller than the volume of the vesicle. The disrupted membrane has defects that are below the microscope resolution power. Probably, their scattering induces extra interference effects responsible for the loss of vesicle contrast observed under the microscope, which are not a simple consequence of the reduced macroscopic refractive index.

At this moment it is only possible to make a speculative guess about the formation and evolution of the perforations. Punctual pores are dynamic entities that do not usually

present a defined correlation. Water fissures in the headgroup region formed by coalescence of cavities and pores may have more stability, giving rise to the observed in-plane correlation. Such fissures may correspond to cavities occurring independently in each of the two membrane surfaces (internal and external monolayer), or to perforations along the full bilayer thickness. This would lead to the picture of a vesicle formed of interconnected fragments with their borders in contact with water pores with curved walls, shown as a cartoon in Fig. 10. The cartoon shows a simple representation, where the vesicle macroscopic shape is maintained. However, the presence of perforations will certainly facilitate vesicle shape deformation, such as formation of angles between fragments and fragment bending.

It has been shown that in the case of circular pores there is a rupture transition separating intact membranes from a disintegrated state (Shillcock and Seifert, 1998). There is a critical pore radius, below which individual pores reseal and above which there is coalescence into a single large hole. Furthermore, instability arises from an increase in small-hole density or fluctuations of hole size (Shillcock and Seifert, 1998). We suggest that the stability of the IP rests on linear coalescence into fissures correlated with localized changes in bilayer thickness occurring in the melting regime.

SAXS results demonstrate that the perforations evolve with temperature. On one hand the IP peak has a better definition and a maximum q_1 at $\sim 25°C$ (Fig. 3 c). On the other hand, the intensity of the bilayer peak, I_{max}, does not change abruptly with T_m^{on}, but has a sharp minimum just below T_m^{off} (Fig. 3 b). The optical data show sharp changes at both T_m^{on} and T_m^{off}. These characteristics indicate a better definition of the fragments in the center, ($\sim 25°C$) possibly with an evolution from cavities in the headgroup region to perforations of the bilayer, as well as oriented coalescence of cavities into fissures. At T_m^{on} punctual pores are enough to allow passage of light with drastic reduction of contrast and turbidity, but do not produce yet much change in the average bilayer structure or in the membrane refractive index. Evolution of fissures produces a better definition of the average fragment size, and evolution of perforations strongly decreases the x-ray contrast. The variation of q_1 with concentration might indicate that the structure of the surface network depends on surface charge fluctuations, which are sensitive to the interactions between neighboring vesicles.

CONCLUSIONS

The SAXS and optical microscopy results presented here, together with other features of the intermediate phase of low ionic strength DMPG dispersions up to 70 mM DMPG, can be consistently explained with a model of disrupted/perforated unilamellar vesicles in the IP. To our knowledge, this is the first report of an in-plane mesoscopic structure connected to membrane defects in a single vesicle, with a defined average correlation length revealed by a peak in the

SAXS region. This model is supported also by the ESR results evidencing the existence of two populations with different mobility in the IP (Riske et al., 2003a).

The DMPG intermediate phase has been proposed previously to correlate with formation of a lipid network, which would have more curvature than the vesicles and would be dependent on particular values of an osmotic driving force defined by solvent-dependent interactions not specified (Schneider et al., 1999). We stress, however, that such network could not be a usual sponge or bicontinuous phase, which have average curvature equal to zero, with segments having both positive and negative curvatures (Porte et al., 1989; Lei et al., 1997). This situation is not favored by the electrostatic repulsion between the polar heads. The model proposed here corresponds to a network on the vesicle surface, having only positive excess curvature, and is able to account for the behavior at the molecular level. Moreover, the strong asymmetry between T_m^{on} and T_m^{off} in the DSC curves, as well as in ESR and SAXS results (Riske et al, 2001) indicates that the effects cannot be simulated by simply imposing different populations in the two monolayer halves of the bilayer, as done in Schneider et al. (1999), since this implies symmetric DSC curves.

The picture of the DMPG melting regime can be summarized as follows. At T_m^{on} density fluctuations destroy the long-range order between hydrocarbon chains. Isolated *gauche* rotations may occur, but there is not yet a decrease in the overall bilayer thickness, which requires a collective rearrangement of the disordered chains, with defined kinks. With such mobility, polar heads separate due to the electrostatic repulsion, allowing penetration of water and possibly ions more deeply into the membrane. The proposal of cavities in the headgroup region, open by density fluctuations connected to the melting transition, has been made previously, as a probable explanation for the existence of a peak in the sodium permeability at T_m in pure phospholipid vesicles (Nagle and Scott, 1978). Such effect would be connected to a peak in the bilayer lateral compressibility near the critical point below T_m. In that case, both cavity formation and chain melting happen concomitantly at T_m. In the case of charged DMPG the process occurs along a melting regime. Pores are formed, which coalesce into stable fissures upon increasing the temperature, while the chain-melting process gradually takes place. The highly curved pore/fissure walls shall be associated with regions of higher surface potential and less counterion binding, due to the increased intermolecular separation caused by electrostatic repulsion (Watts et al., 1978). At T_m^{off} the integrity of the membrane surface is restored, with collective rearrangement of the hydrocarbon chains in a compact fluid state of smaller thickness.

The opening of aqueous pores and/or disruption defects within the melting regime is likely to have biological relevance. Phosphatidylglycerols are the most abundant anionic phospholipids present in prokaryotic cell mem-
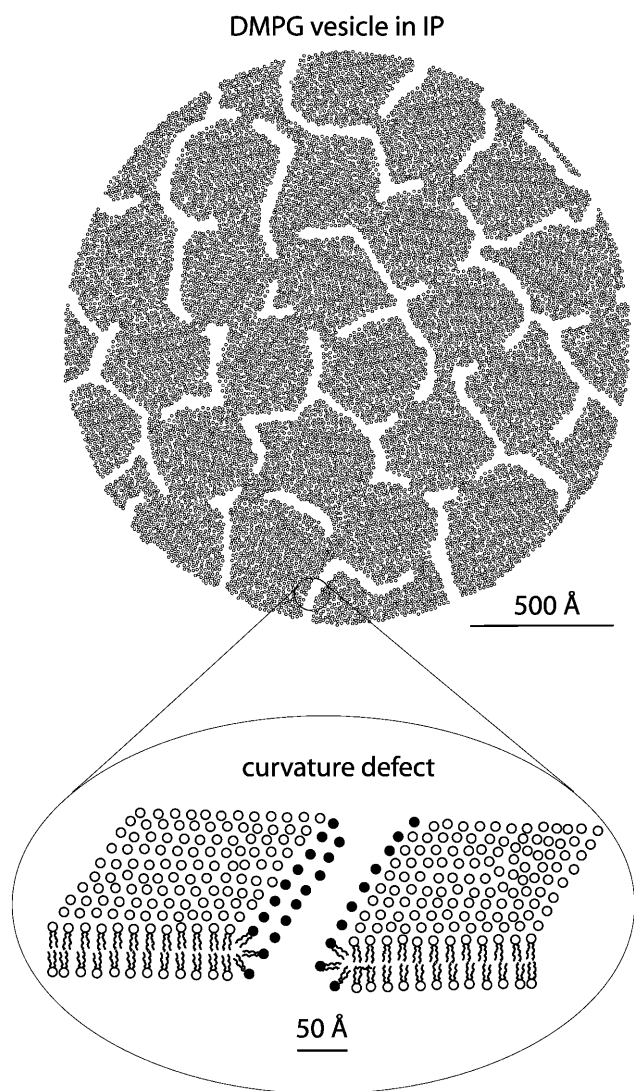
DMPG vesicle in IP

FIGURE 10 Cartoon of the proposed mesoscopic structure in the IP. On top, a DMPG vesicle composed of bilayer pieces is depicted. The bar indicates the order of magnitude of the vesicle size (radius = ~1000 Å; fragment size = ~400 Å). The open regions do not correspond necessarily to channels perforating the full bilayer, but may also be fissures in only one monolayer. In this cartoon the vesicle surface remains smooth, but most probably the curvature defects induce changes in vesicle topology, and angles between fragments and/or bending of fragments are expected to occur. Shown in the bottom is a zoom at the edge of one perforation. The headgroups painted in black correspond to highly curved DMPG molecules. The bar indicates 50 Å, about the bilayer thickness.

branes. Furthermore, this behavior might be a characteristic of charged membranes in general. A high local concentration of charged lipids could help the formation/stabilization of transient pores across the membrane, which would enable a controlled material transport across biological membranes. The presence of disruption defects could also facilitate biological processes involving changes in membrane topology. An example is the Golgi apparatus, which is composed of bilayer stacks and vesicles, and which has to break up into a set of smaller fragments and vesicles during

mitosis. Therefore, basic research on membrane phase transitions involving topological changes connected to changes in charge density is of clear biological relevance.

Furthermore, one can envision technological applications, where a controlled opening of pores as a response to changes in external conditions, such as temperature, ionic strength, and pH, could be used in targeted drug delivery.

REFERENCES

Angelova, M. I., and D. S. Dimitrov. 1986. Liposome electroformation. *Faraday Discuss. Chem. Soc.* 81:303–311.

Bagatolli, L. A., and E. Gratton. 2000. A correlation between lipid domain shape and binary phospholipid mixture composition in free standing bilayers: a two-photon fluorescence microscopy study. *Biophys. J.* 79:434–447.

Cevc, G. 1993. Phospholipid Handbook. Marcel Dekker, New York.

Chernik, G. G. 1995. Phase-equilibria in phospholipid water-systems. *Adv. Coll. Interf. Sci.* 61:65–129.

Cummins, H. Z., and A. P. Levanyuk, editors.1983. Light Scattering Near Phase Transitions. North-Holland, Amsterdam, The Netherlands.

Epand, R. M., and S. W. Hui. 1986. Effect of electrostatic repulsion on the morphology and thermotropic transitions of anionic phospholipids. *FEBS Lett.* 209:257–260.

Epand, R. M., B. Gabel, R. F. Epand, A. Sem, and S. W. Hui. 1992. Formation of a new stable phase of phosphatidylglycerol. *Biophys. J.* 63:327–332.

Gershfeld, N. L., W. F. Stevens, Jr., and R. J. Nossal. 1989. Equilibrium studies of phospholipid bilayer assembly. Coexistence of surface bilayers and unilamellar vesicles. *Faraday Discuss. Chem. Soc.* 81:19–28.

Glaser, R. W., S. L. Leikin, L. V. Chernomordik, V. F. Pastushenko, and A. I. Sokirko. 1988. Reversible electrical breakdown of lipid bilayers—formation and evolution of pores. *Biochim. Biophys. Acta.* 940:275–287.

Glatter, O., and O. Kratky, editors.1982. Small Angle X-Ray Scattering. Academic Press, New York.

Heimburg, T., and R. L. Biltonen. 1994. Thermotropic behavior of dimyristoylphosphatidylglycerol and its interaction with cytochrome c. *Biochemistry.* 33:9477–9488.

Hura, G., D. Russo, R. M. Glaeser, T. Head-Gordon, M. Krack, and M. Parrinello. 2003. Water structure as a function of temperature from x-ray scattering experiments and ab initio molecular dynamics. *Phys. Chem. Chem. Phys.* 5:1981–1991.

Koynova, R., and M. Caffrey. 1998. Phases and phase transitions of the phosphatidylcholines. *Biochim. Biophys. Acta.* 1376:91–145.

Lamy-Freund, M. T., and K. A. Riske. 2003. The peculiar thermo-structural behavior of the anionic lipid DMPG. *Chem. Phys. Lipids.* 122:19–32.

Lei, N., C. R. Safinya, D. Roux, and K. S. Liang. 1997. Synchrotron x-ray-scattering studies on the sodium dodecyl sulfate-water-pentanol-dodecane L-3 sponge phase. *Phys. Rev. E.* 56:608–613.

Luzzati, V. 1968. X-ray diffraction studies of lipid-water systems. *In* Biological Membranes. D. Chapman, editor. Academic Press, New York. 71–123.

Mason, P. C. 1988. Mixing behavior of symmetric chain-length and mixed chain-length phosphatidylcholines in 2-component multilamellar bilayers—evidence for gel and liquid crystalline phase immiscibility. *Biochemistry.* 27:4421–4429.

Mason, P. C., B. D. Gaulin, R. M. Epand, and J. Katsaras. 2000. Critical swelling in single phospholipid bilayers. *Phys. Rev. E.* 61:5634–5639.

Nagle, J. F. 1980. Theory of the main lipid bilayer phase-transition. *Annu. Rev. Phys. Chem.* 3:157–195.

Nagle, J. F., H. I. Petrache, N. Gouliaev, S. Tristram-Nagle, Y. Liu, R. Suter, and K. Gawrish. 1998. Multiple mechanisms for critical behavior in the biologically relevant phase of lecithin bilayers. *Phys. Rev. E.* 58:7769–7776.

Nagle, J. F., and H. L. Scott, Jr. 1978. Lateral compressibility of lipid mono- and bilayers. Theory of membrane permeability. *Biochim. Biophys. Acta.* 513:236–243.

Nagle, J. F., and S. Tristram-Nagle. 2000. Structure of lipid bilayers. *Biochim. Biophys. Acta.* 1469:159–195.

Nagle, J. F., and D. A. Wilkinson. 1978. Density measurements and molecular interactions. *Biophys. J.* 23:159–175.

Nagle, J. F., R. Zhang, S. Tristram-Nagle, W. Sun, and H. I. Petrache. 1996. X-ray structure determination of fully hydrated L_α-phase dipalmitoyl-phosphatidylcholine bilayers. *Biophys. J.* 70:1419–1431.

Paz, L., J. M. Di Meglio, M. Dvolaitzky, R. Ober, and C. Taupin. 1984. Highly curved defects in lyotropic (nonionic) lamellar phases. Origin and role in hydration process. *J. Phys. Chem.* 88:3415–3418.

Photinos, P. J., and A. Saupe. 1984. Calculations on the electric-conductivity of a lyotropic mesophase with perforated lamellae. *J. Chem. Phys.* 81:563–566.

Porte, G., J. Appell, P. Bassereau, and J. Marignan. 1989. L-alpha to L3—a topology-driven transition in phases of infinite fluid membranes. *J. Phys. Fr.* 50:1335–1347.

Quist, P.-O., and B. Halle. 1993. Curvature defects in a lamellar phase revealed by nuclear-spin-relaxation anisotropy. *Phys. Rev. E.* 47:3374–3395.

Riske, K. A., L. Q. Amaral, and M. T. Lamy-Freund. 2001. Thermal transitions of DMPG bilayers in aqueous solution: SAXS structural studies. *Biochim. Biophys. Acta.* 1511:297–308.

Riske, K. A., H.-G. Döbereiner, and M. T. Lamy-Freund. 2002. Gel-fluid transition in dilute versus concentrated DMPG aqueous dispersions. *J. Phys. Chem. B.* 106:239–246.

Riske, K. A., H.-G. Döbereiner, and M. T. Lamy-Freund. 2003b. Comment on ''gel-fluid transition in dilute versus concentrated DMPG aqueous dispersions.'' *J. Phys. Chem. B.* 107:5391–5392.

Riske, K. A., R. M. Fernandez, O. R. Nascimento, B. L. Bales, and M. T. Lamy-Freund. 2003a. DMPG gel-fluid thermal transition monitored by a phospholipid spin labeled at the acyl chain end. *Chem. Phys. Lipids.* 124:69–80.

Riske, K. A., O. R. Nascimento, M. Peric, B. Bales, and M. T. Lamy-Freund. 1999. Probing DMPG vesicle surface with a cationic aqueous soluble spin label. *Biochim. Biophys. Acta.* 1418:133–146.

Riske, K. A., M. J. Politi, W. F. Reed, and M. T. Lamy-Freund. 1997. Temperature and ionic strength dependent light scattering of DMPG dispersions. *Chem. Phys. Lipids.* 89:31–44.

Salonen, I. S., K. K. Eklund, J. A. Virtanen, and P. K. J. Kinnunen. 1989. Comparison of the effects of NaCl on the thermotropic behaviour of *sn*-1′ and *sn*-3′ stereoisomers of 1,2-dimyristoyl-*sn*-glycero-3-phos-phatidylglycerol. *Biochim. Biophys. Acta.* 982:205–215.

Schneider, M., D. Marsh, W. Jahn, B. Kloesgen, and T. Heimburg. 1999. Network formation of lipid membranes: triggering structural transitions by chain melting. *Proc. Natl. Acad. Sci. USA.* 96:14312–14317.

Shillcock, J. C., and U. Seifert. 1998. Thermally induced proliferation of pores in a model fluid membrane. *Biophys. J.* 74:1754–1766.

Silvius, J. R. 1986. Solid-phase and liquid-phase equilibria in phosphati-dylcholine phosphatidylethanolamine mixtures. A calorimetric study. *Biochim. Biophys. Acta.* 857:217–228.

Van Dijck, P. W. M., A. J. Kaper, H. A. J. Oonk, and J. Degier. 1977. Miscibility properties of binary phosphatidylcholine mixtures. A calorimetric study. *Biochim. Biophys. Acta.* 470:58–69.

Watts, A., K. Harlos, W. Maschke, and D. Marsh. 1978. Control of the structure and fluidity of phosphatidylglycerol bilayers by pH titration. *Biochim. Biophys. Acta.* 510:63–74.

Wiener, M. C., G. I. King, and S. H. White. 1991. Structure of a fluid dioleoylphosphatidylcholine bilayer determined by joint re-finement of x-ray and neutron diffraction data. I. Scaling of neutron data and the distribution of double bonds and water. *Biophys. J.* 60:568–576.

Wiener, M. C., R. M. Suter, and J. F. Nagle. 1989. Structure of the fully hydrated gel phase of dipalmitoylphosphatidylcholine. *Biophys. J.* 55:315–325.

Zhang, Y. P., R. N. A. H. Lewis, and R. N. McElhaney. 1997. Calorimetric and spectroscopic studies of the thermotropic phase behaviour of the *n*-saturated 1,2-diacylphosphatidylglycerols. *Biophys. J.* 72:779–793.